



## RESEARCH ARTICLE

10.1002/2017EF000678

# Investigation of Changes in Extreme Temperature and Humidity Over China Through a Dynamical Downscaling Approach

Jinxin Zhu<sup>1</sup>, Gordon Huang<sup>2</sup>, Xiuquan Wang<sup>3</sup>, and Guanhui Cheng<sup>1</sup>**Key Points:**

- Robust projects of combined extreme temperatures and relative humidity over China
- combination effects of high-temperatures and relative humidity are substantially smaller than generally anticipated for China.
- Projected increases in frequencies and duration of high-temperature extremes in China

**Correspondence to:**Gordon Huang, [huang@iseis.org](mailto:huang@iseis.org)**Citation:**

Zhu, J., Huang, G., Wang, X., & Cheng, G. (2017). Investigation of Changes in Extreme Temperature and Humidity Over China Through a Dynamical Downscaling Approach, *Earth's Future*, 5, 1136–1155, <https://doi.org/10.1002/2017EF000678>

Received 13 SEP 2017

Accepted 15 OCT 2017

Accepted article online 1 NOV 2017

Published online 23 NOV 2017

<sup>1</sup>Faculty of Engineering and Applied Science, University of Regina, Regina, Saskatchewan, Canada, <sup>2</sup>Institute for Energy, Environment and Sustainable Communities, University of Regina, Regina, Saskatchewan, Canada, <sup>3</sup>School of Geosciences, University of Louisiana at Lafayette, Lafayette, LA, USA

**Abstract** Impacts of climate change relating to public health are often determined by multiple climate variables. The health-related metrics combining high-temperature and relative humidity are most concerned. Temperatures, relative humidity and relationship among them are investigated here for a comprehensive assessment of climate change impacts over China. A projection of combined temperatures and humidity through the PRECIS model is addressed. The PRECIS model's skill in reproducing the historical climate over China was first gauged through validating its historical simulation with the observation data set in terms of the two contributing variables. With good results of validation, a plausible range of combined temperatures and relative humidity were generated under RCPs. The results suggested that the annual mean temperature of China will increase up to 6°C at the end of 21st century. Opposite to the significantly change in the temperature, the maximum magnitude of changes in relative humidity is only 8% from the value in the baseline period. The dew point temperature is projected to be 14.9°C (within the comfortable interval) over the whole nation under high radiative forcing scenario at the end of this century. Therefore, the combination effects of high temperatures and relative humidity are substantially smaller than generally anticipated for China. Even though the impact-relevant metric like the dew point temperature is not projected as bad as the generally anticipated, we found that the frequency of high-temperature extremes increases up to 40% and the duration increases up to 150% in China. China is still expected to have more number of extremely hot days, more frequent high-temperature extremes, and longer duration of warm spell than before. Regionally, South China has the smallest changes in the mean, maximum and minimum temperatures while the largest increases in all five high-temperature indices. Consequently, the climate over South China for two future periods will be changing more drastically than the baseline period. Extra cautions need to be given to South China in the future.

## 1. Introduction

China was experiencing more frequency and intensity of extreme temperature events than before in the past 10 years (Chen et al., 2015; Chen & Zhou, 2017; Ding et al., 2010; Fang et al., 2008; Fang et al., 2015; Li et al., 2017; Ren & Zhou, 2014). In detail, analysis based on longer data records showed that the hot days and heat waves events sharply increased by more than 10% over China in the last decade (Ding et al., 2010). Studies for mainland China also suggested a countrywide increase in frequency of hot events and warm days (nights). For example, Ren and Zhou's research indicated that annual highest daily maximum temperature and daily minimum temperature increased across the country. Their results also showed that warm nights (days) significantly increased at a rate of 8.16 days (5.22 days) over the whole nation for the past 10 years (Ren & Zhou, 2014). Temperature is one of the most important climate variables with regard to human comfort, and excessively high temperatures account for more fatalities than lightening, floods, tornadoes, and hurricanes do in China (Lin et al., 2016; Ma et al., 2017; Wang et al., 2015b). But the effects of high-temperature extremes can be compounded by other factors, such as the air pollution, intensity of sunlight, strength of wind and humidity. Particularly, the humidity can be combined with high temperatures to create some indices such as apparent temperature, heat index, and dew point temperature (Isaac & van Wijngaarden, 2012). Such indices account for temperatures that can be perceived by the human body. One of the human

© 2017 The Authors.

This is an open access article under the terms of the Creative Commons Attribution-NonCommercial-NoDerivs License, which permits use and distribution in any medium, provided the original work is properly cited, the use is non-commercial and no modifications or adaptations are made.

body's effective mechanisms in guarding against excessive heat is perspiration. Perspiration cools the body because the process of sweat evaporating into the atmosphere consumes latent heat. If the atmosphere has a high humidity, the rate of evaporation process is retarded and loss of latent heat is reduced. This results in the threat of heat stroke (a potentially fatal caused by increase in the body's internal temperature) faced by people. Therefore, useful guidelines can be provided for people by studying the combination of heat and humidity. To this end, temperature and humidity are considered as well-established risk factors for human health under climate change. For a comprehensive assessment of the combination impacts under climate change, it is imperative to take into account for the uncertainties in both contributing variables. It is well understood that the different variables can be linked through first principles or basic mechanisms. For instance, the Clausius–Clapeyron (C-C) equation illustrates that saturation vapor pressure increases exponentially with temperature (Sperber et al., 2013). In the other word, warmer air is able to hold more moisture. Despite the knowledge about the relationship between temperature and humidity, it is often ignored in the context of projection. For example, the Fifth Assessment Report of the Intergovernmental Panel on Climate Change provides projections of many variables including temperature and humidity, but each of them is analyzed and discussed separately.

Some recent studies have quantified how relationships across variables evolve into the future. Beniston analyzed the trends in joint quantiles of temperature and precipitation in Europe since 1901 and projected them for 2100 (Beniston, 2009). Utsumi et al. investigated the applicability of the C-C relation to the scaling relationship between extreme precipitation intensity and surface air temperature (Utsumi et al., 2011). There are also some studies having quantified how often-correlated uncertainties in the relationships can be transformed into joint probabilistic projections. Watterson calculated joint PDFs for climate change with properties matching Australian projections (Watterson & Whetton, 2011). Tebaldi and Sanso applied a hierarchical Bayesian approach to obtain the joint projections of temperature and precipitation change from multiple climate models (Tebaldi and Sanso, 2009). Fischer and Knutti used simulations from 15 general circulation models (GCMs) of the new Climate Model Intercomparison Project phase 5 to demonstrate that models projecting greater warming also show a stronger reduction in relative humidity (RH) and uncertainties in some impact-relevant metrics such as extremes of health indicators are substantially smaller than generally anticipated. However, two drawbacks can be concluded from the previous researches (Fischer & Knutti, 2013). First, few researches have been carried out to address joint projections in temperature and humidity which are considered as well-established risk factors for human health. Second, for existing researches on projecting temperature and humidity, there is no Regional Climate Models (RCMs) but GCMs having been applied to address the joint projection in these two variables. However, GCMs assume that RH stays constant and will increase at a rate of approximately 6.8%/°C as indicated by the C-C relationship. Substantial researches have found that the assumption of constant RH does not hold across all temperatures. Specially, our recent study on investigating the relationship between extreme sub-daily precipitation and surface temperature in China has revealed that RCMs with a closure of the convection scheme based on moisture convergence can better simulate the relationship than GCMs (Zhu et al., 2017). We will elaborate on this in the following section.

The objective of this study is to address projections of combined temperature extremes and humidity through a RCM. The selected RCM's skill in reproducing the historical climate over China will be gauged through validating its historical simulation with the observation dataset in terms of temperatures and RH. Particularly, the simulated relationship across two variables will be examined for addressing the joint behavior of uncertainties. After the validation, the independent climate variables will be projected from the dynamical downscaling under different greenhouse gas emission scenarios. Projections will be combined to quantify how the relationship between the two variables evolves under climate change. Eventually, the impacts of climate change on temperature extremes and RH can be assessed comprehensively by considering the joint behavior of uncertainties.

## 2. Models, Experimental Design, and Data

The RCM used in this study is the PRECIS model developed by UK Met Office Hadley Centre (Jones et al., 2004; Wilson et al., 2015). It is an atmospheric and land surface model of limited area and high resolution which is originally designed to operational forecast and satisfy atmospheric research needs. It describes dynamical flow, the atmospheric sulfur cycle, clouds and precipitation, radiative processes, the land surface, and the

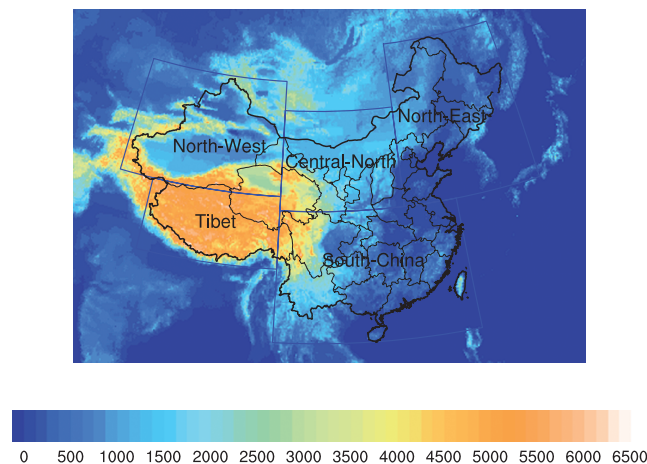


**Figure 1.** Model domain, topography (m), and the five subregions: Northwest, Northcentral, Northeast, Tibet, and South.

dynamically downscaled for the high-resolution historical and future climate (Collins et al., 2008). The HadGEM2-ES climate model comprises an atmospheric GCM at N96 and L38 horizontal and vertical resolution, and an ocean GCM with a 1° horizontal resolution (increasing to 1/3° at the equator) and 40 vertical levels. This model has also been validated that it has the ability in simulating climate over China (Yan et al., 2015).

The computational domain of PRECIS simulation is centered at (34°N, 105°E), and it covers China with 292 × 186 horizontal grid points and a lateral buffer zone of eight grid points. The spatial resolution is 0.22° × 0.22°. The PRECIS model runs continuously from 1969 to 2005 for the historical simulation and from 2006 to 2099 for the future projections. Future simulations are forced with specified concentrations consistent with a medium emission scenario (RCP4.5) and a high emission scenario (RCP8.5). RCP4.5 is a stabilization scenario, with the total radiative forcing of 4.5 W/m<sup>2</sup> until 2100. RCP8.5 is a scenario of comparatively high greenhouse gas emissions with stabilizing near 8.5 W/m<sup>2</sup> (Hewitson et al., 2014; Moss et al., 2010). With these two RCP scenarios, changes in temperature can be investigated under increasing radiative forcing.

To further investigate the geographical features of temperature changes, we divide the contiguous China domain into five subregions which are in accordance with the Third China's National Assessment Report on Climate Change (Wang & Zheng, 2012). As shown in Figure 1, five subregions are Northwest China, Northcentral China, Tibet, Northeast China, and South China. For each subregion, we calculate the area-averaged temperature change and obtain the differences in the mean and extreme temperature of all five subregions. The temperature indices can be divided into two main categories, namely low- and high-temperature indices. As the objective of this study is to investigate the combination effects of temperature and humidity. The combination effects are effective when high temperature is compounded by humidity. Therefore, five high-temperature indices are used in this study and have been described in detail in Table 1 (Frich et al., 2002). To assess the skills of model simulations of the historical climate, observational data are needed as references to compare with the model results. The observed mean, maximum, and minimum temperatures are from the Climate Research Unit (CRU) monthly gridded data set with a spatial resolution of 0.5° × 0.5°. The CRU data set is based on the interpolation from monthly observations at meteorological stations across the world's land areas and covers a period of more than 50 years (Harris et al., 2014). It applies enhancement of quality control algorithm to develop the global climate variables products highly resolved in time and space. As CRU is a monthly observational data set, it cannot be used to calculate the temperature indices. Daily maximum and minimum temperature data from Chinese National Meteorological Center are adopted to derive the five selected indices to validate the dynamically downscaled simulation (as shown in Figure 2). Data from 202 stations is selected from 726 stations for analysis after passing the spatial and temporal consistency test (Feng et al., 2004).

deep soil. The PRECIS model has been widely applied in regional climate simulations (Feng et al., 2012; Wang et al., 2014, 2015a; Xu et al., 2006), and its ability in simulating climatological mean and extreme climate over China has been tested and verified (Xu et al., 2009). Moreover, PRECIS exhibits improvements in its simulating performance of the inter-annual variations presented by the driving data (Wang et al., 2015a).

The HadGEM2-ES (Hadley Centre Global Environment Model version 2 – Earth Systems) provides the meteorological forcing at the boundaries of the PRECIS model's domain as its Lateral Boundary Conditions to be

**Table 1.**  
*Definitions of Extreme Temperature Indices Used in This Study*

Labels	Name	Index definition	Units
<b>SU</b>	Summer days per period	The counted number of days where the daily maximum temperature great than 25°C	1
<b>TR</b>	Tropical nights index per period	The counted number of days where the daily minimum temperature great than 20°C	1
<b>TN90p</b>	Percentage of days when TN > 90th percentile	The percentage of time where daily minimum temperature is great than the 90th percentile of daily minimum temperature for the reference period	%
<b>TX90p</b>	Percentage of days when TX > 90th percentile	The percentage of time where daily maximum temperature is great than the 90th percentile of daily maximum temperature for the reference period	%
<b>HWFI</b>	Warm spell days	Annual count of days with at least 6 consecutive days when the daily maximum temperature is great than 90th percentile	1

### 3. Simulations of Historical Temperature and Humidity

Figure 3 shows the spatial distribution of annual mean, maximum, and minimum temperature over China derived from HadGEM2-ES, PRECIS, and CRU for the period from 1976 to 2005. The figure of CRU shows that annual mean temperature is relatively low over Tibet, increasing southeastward and reaching the maximum in South China. The annual maximum and minimum temperatures also exhibit similar spatial distribution. Comparing to CRU, HadGEM2-ES simulates the annual mean temperature in a similar spatial pattern, the temperature increasing southeastward. However, the simulated temperature is higher than the observations' over Tibetan Plateau and Northeast China. There is an overestimation of annual maximum temperature and an underestimation of annual minimum temperature over the whole China except South China. The nonuniform between simulated temperature and observation is a common occurrence in many other GCMs with a coarse resolution (Cheng et al., 2017; Flato et al., 2013; Zhou et al., 2013). PRECIS significantly eliminates its occurrences and reproduces better spatial patterns for annual mean, maximum, and minimum temperatures. PRECIS captures the warm observational center locating in South China and Northwest China, and the cold center in Tibetan Plateau for both days and nights.

To gauge the skills of HadGEM2-ES and PRECIS in reproducing the annual mean, maximum, and minimum temperatures, the Taylor Diagram is introduced to summarize how closely the patterns from two models' results match the observation (Taylor, 2001). It exhibits the correlation coefficient (COR), standard deviation (SD), and root-mean-square error (RMSE) between simulated patterns and the observational pattern in a graphical way. The simulated pattern with the right amplitude of its variations (represented by SD), high correlation, and low RMSE agrees well with the observation. On the plot, the pattern will have a closer distance to the reference point marked "OBS" on the x-axis. Figure 4 shows the relative merits of HadGEM2-ES and PRECIS with respect to reproducing the spatial patterns of annual mean, maximum and minimum temperature for China and its five subregions. All results from PRECIS have CORs greater than 0.95, and SDs between 0.9 and 1.1 for China, while results from HadGEM2-ES have smaller CORs and wider spread SDs between 0.8 and 1.2 than PRECIS. It indicates that PRECIS has a relatively high skill of reproducing the spatial distribution of mean temperature over China for both days and nights. As for the five subregions, the performance of PRECIS outweighs HadGEM2-ES in every subregion, but PRECIS shows an inconsistent performance level in the different subregion. Results of PRECIS have the lowest CORs and highest RMSEs over Northwest China compared with the results of other four regions. The relatively poor performance of PRECIS over this subregion could be caused by its driving GCM since HadGEM2-ES, here, simulates the highest RMSE and SD among all five subregions. Simulated patterns of PRECIS over South China agree best with the observation as their points have the shortest distances to the reference point in the plot. The relatively high skill of PRECIS in simulating spatial patterns may relate to the inputs of its driving GCM because the performance of HadGEM2-ES over South China is also the best among all five subregions. Overall, it is evident that PRECIS outperforms HadGEM2-ES, and the performance of HadGEM2-ES affects the skill of PRECIS

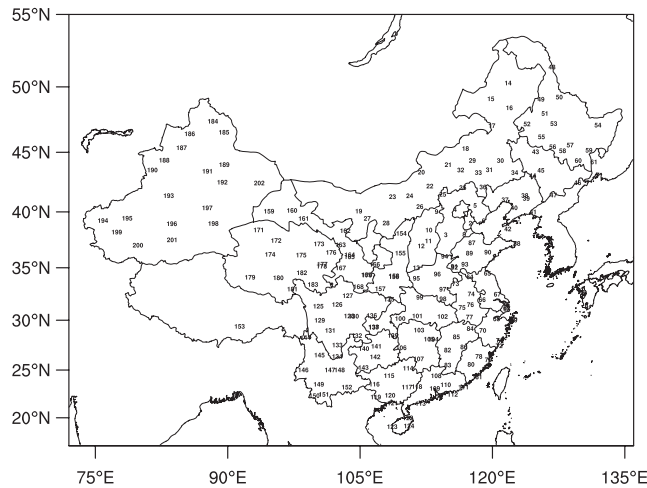


**Figure 2.** Spatial distribution of selected stations for analysis in China.

2.3°C for the annual minimum temperature. In northern subregions (Central North, Northwest, and Northeast China), HadGEM2-ES tends to overestimate the annual mean, maximum, and minimum temperature in June, July, and August, namely the temperature in summer, and underestimate the temperature as large as 6°C in winter (December, January, and February). Annual cycles of PRECIS are also above the curves of observation in summer for all three temperature indices. As for other three seasons, the results of PRECIS, however, better agree with CRU than results of its driving GCM. In South China, both models' values generally stick together and are closer to the observation's except that the annual cycle of HadGEM2-ES is about 1°C under the observation of the annual minimum temperature. In Tibet, results of HadGEM2-ES exhibit overestimation for both the annual mean and maximum temperature, and underestimation for the annual minimum temperature. The curve of HadGEM2-ES is about 5°C above the observation for the annual maximum temperature, and is about 3°C below the reference curve for the annual minimum temperature. As for the results of PRECIS, they only have some underestimations in winter and spring for the annual mean temperature. Other than that, they match with the observation better than HadGEM2-ES for all three indices. Based on the results above, PRECIS is more reliable than HadGEM2-ES to represent the annual cycles for China and all five subregions.

In Figure 6, simulated indices of temperature extremes (SU, TR, TN90, and TX90) from HadGEM2-ES and PRECIS are validated with indices derived from the observational data from selected stations for the baseline period. Per definition, the indices (TN90p, TX90p, and HWFI) are calculated by referring to the 90th percentile of the daily maximum and minimum temperature for the baseline period. Therefore, it is necessary to validate these thresholds for extreme temperature indices with the observation data set. For each chart, it takes into account of the daily temperature data of every grid cell in the selected region for the analysis. Each column represents the mean value of the selected index calculated from all grids' temperature in a sub-region for 30 years. For China, values of PRECIS match with the values of the observation in respect to the four selected extreme indices. HadGEM2-ES, on the other side, underestimates all indices. For all five subregions, both models can capture the geographical differences for most indices. For example, PRECIS can eliminate these unrealistic occurrences and gives the highest or lowest values in the right subregions for all indices. Therefore, it is unequivocal that PRECIS, with finer scale physical process simulation, can better depict the distributions of extreme temperature events than HadGEM2-ES simulation does for China. It is further proved that high-resolution simulation is essential to obtain the plausible distribution of temperature over China. A faithful reproduction of historical climate is the premise for projecting a plausible range of future climate.

To validate the skill of the PRECIS model in simulating the historical RH, we used the monthly vapor pressure data from CRU and converted the vapor pressure to RH. The RH was computed from the observed vapor pressure ( $e$ ) and temperature as follows. First, the saturation vapor pressure ( $e_s$ ) at a temperature ( $T$ ) was

in respect of simulating the spatial distributions of annual mean, maximum and minimum temperature for China and five subregions.

Figure 5 demonstrates the annual cycles of temperature estimated from two models' outputs and the observational data for China and five subregions. For China, the curve of PRECIS well matches the annual cycle of CRU for annual mean, maximum, and minimum temperatures. Though HadGEM2-ES does capture the trends of the observed annual cycle, it holistically overestimates around 1.7°C for the annual mean temperature and about 2.1°C for the annual maximum temperature, and underestimates

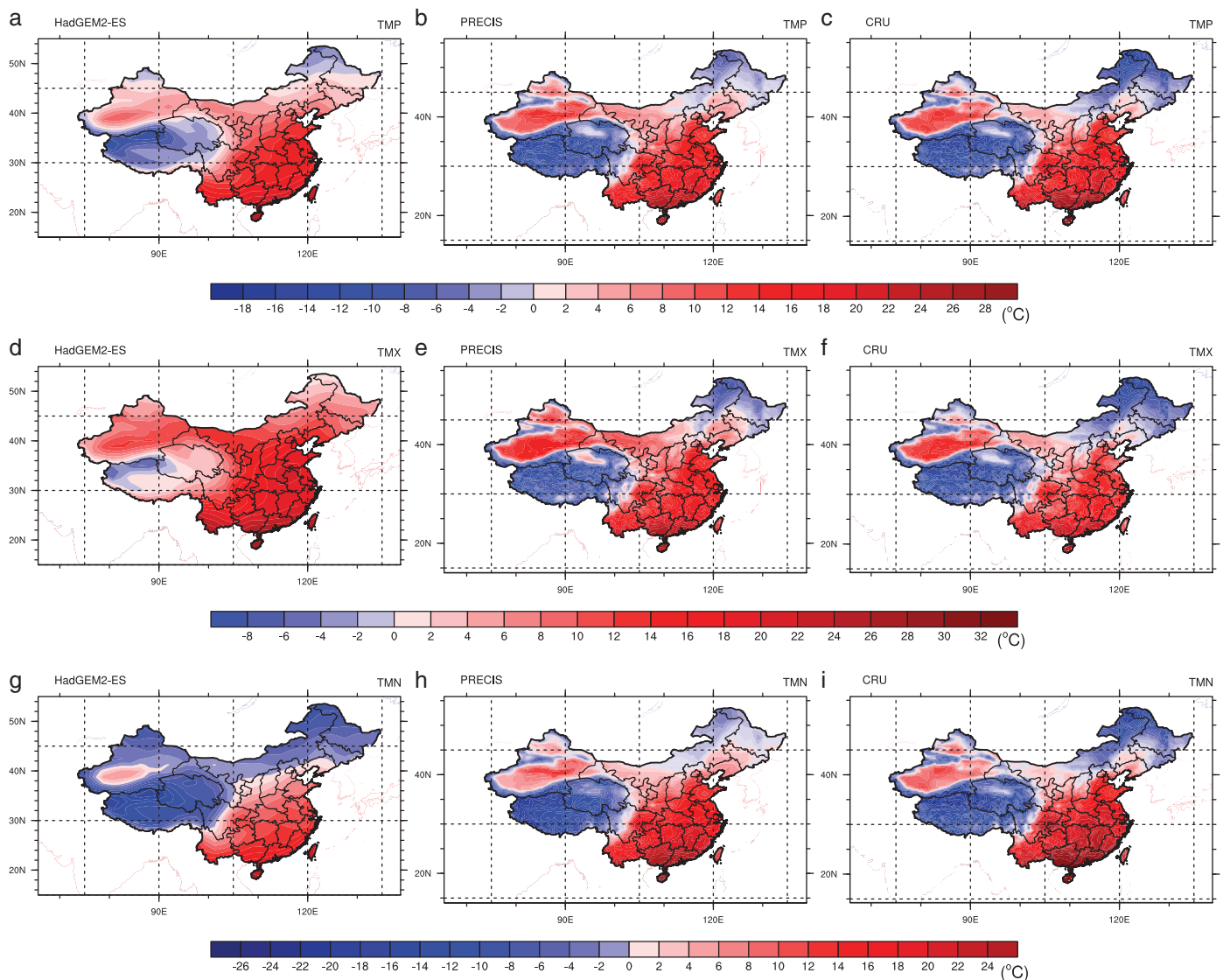


**Figure 3.** Spatial distributions of mean (TMP), maximum (TMX) and minimum (TMN) temperature (°C) over China from HadGEM2-ES (a, d, and g), PRECIS (b, e, and h), and observations (CRU) (c, f, and i) for 1976–2005.

measured by the conversion equation from the Goff–Gratch vapor pressure formula (Goff & Gratch, 1946; List, 2000; Murray, 1967). This formula is valid for temperatures between  $-45$  and  $60^{\circ}\text{C}$ . The RH was obtained by dividing the saturation vapor pressure by the observed vapor pressure.

$$e_s(T) = 6.112e^{17.62T/(243.12+T)}$$

$$RH = 100 \times \left( \frac{e}{e_s} \right)$$

After converting the observed vapor pressure to RH, each model's output was validated with the observation data set regarding the annual mean RH. As shown in Figure 7, the observation shows that the annual mean RH is relative low in northwest China, increasing southeastward. Comparing to CRU, HadGEM2-ES overestimates the RH all over the nation and simulates an artificial high RH area over Tarim Basin in northwest China. The PRECIS model successfully eliminates this overestimation and faithfully reproduces the high

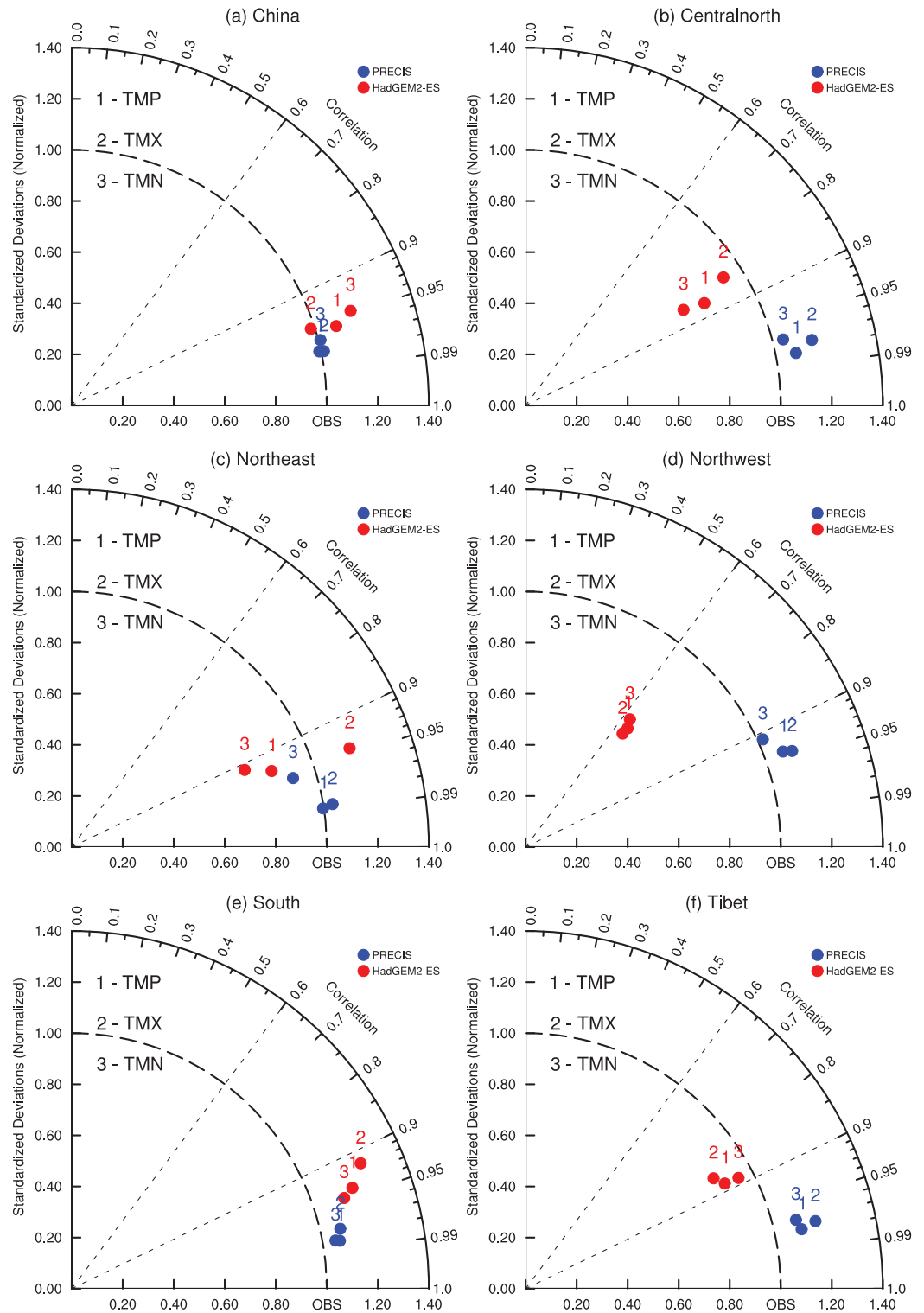


**Figure 4.** Comparison of model simulations of mean (TMP), maximum (TMX) and minimum (TMN) temperature over China and five subregions in Taylor diagrams for 1976–2005. (a) China, (b) Centralnorth, (c) northeast, (d) northwest, (e) South, (f) Tibet

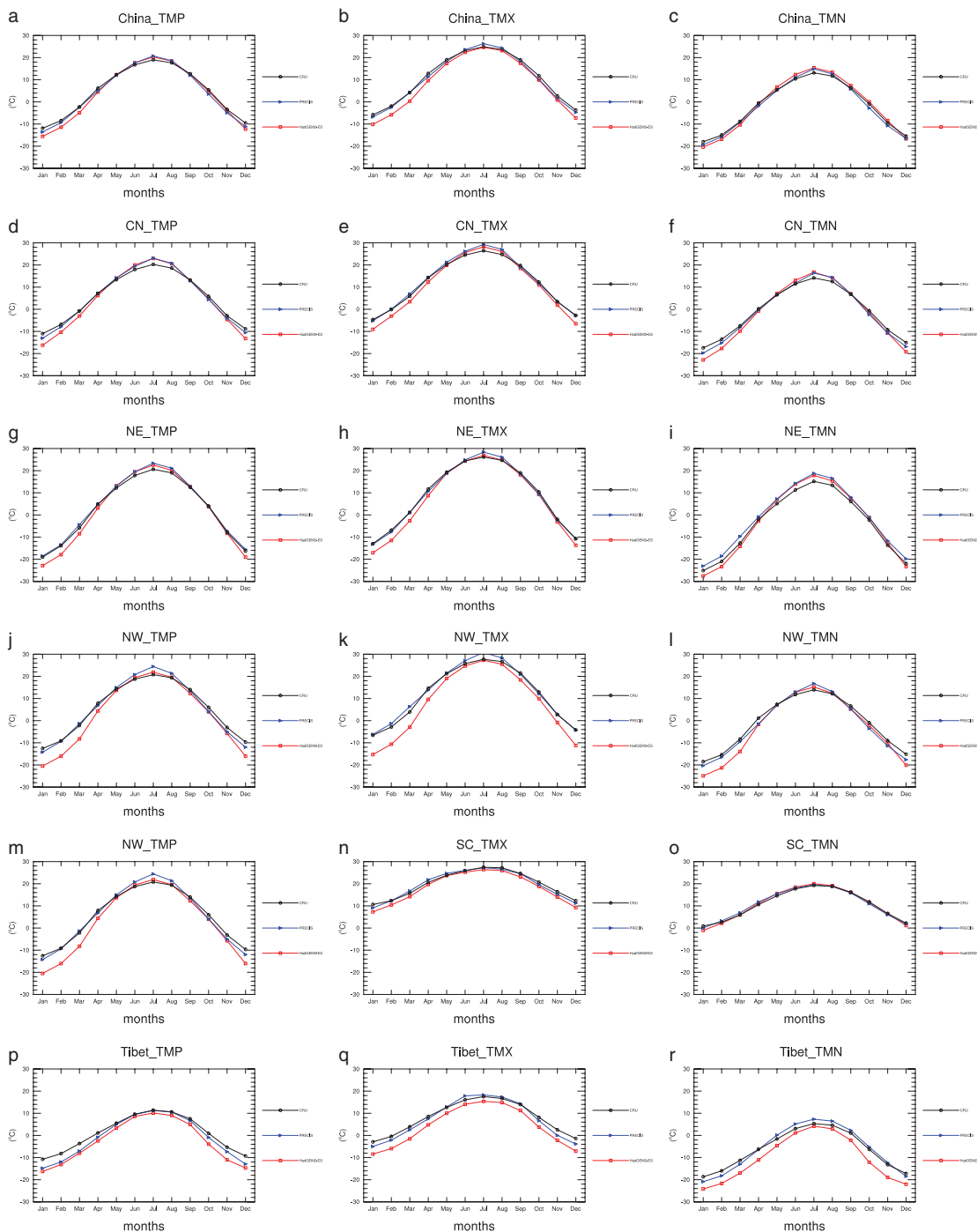
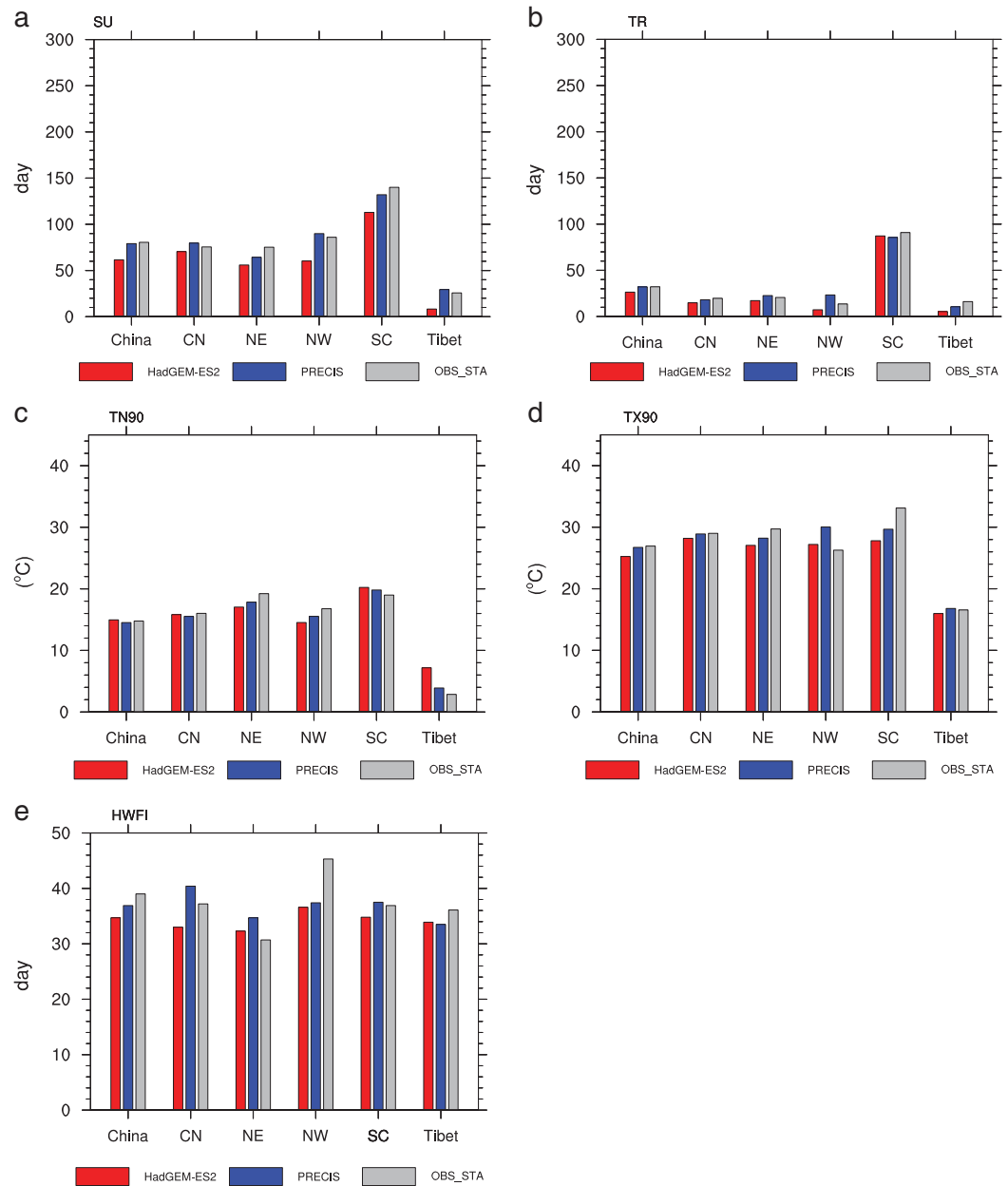


Figure 5. Annual cycle of mean (TMP), maximum (TMX) and minimum (TMN) temperature (°C) over China (a–c) and its five subregions (d–r) during 1976–2005.



**Figure 6.** Regional averages for indices of annual mean temperature extreme (SU, day; TR, day; TN90, °C; TX90, °C; HWFI, day) over China for HadGEM2-ES, PRECIS, and observations from 1976 to 2005.

humidity center in the southwest China. PRECIS captures the warm observational center locating in South China and Northwest China, and the cold center in Tibetan Plateau for both days and nights. In addition, the PRECIS model simulates more reliable spatial distributions and closer magnitude of RH in China.

In the Introduction section, we mentioned that the PRECIS model with a closure of the convection scheme based on moisture convergence can better simulate the relationship between extreme subdaily precipitation and surface temperature in China than its driving GCM. GCMs predict an exponentially increase in extreme precipitation intensity with temperature increasing in the absence of moisture limitation. Observations suggest that there is a negative scaling of extreme precipitation with high temperatures. Our previous study found that the PRECIS model simulated a peak structure in the curve relating daily precipitation extremes with local temperatures. The curve increases at a rate determined by the C-C relationship at the low-medium range of temperature variations but decreases at high temperatures. The

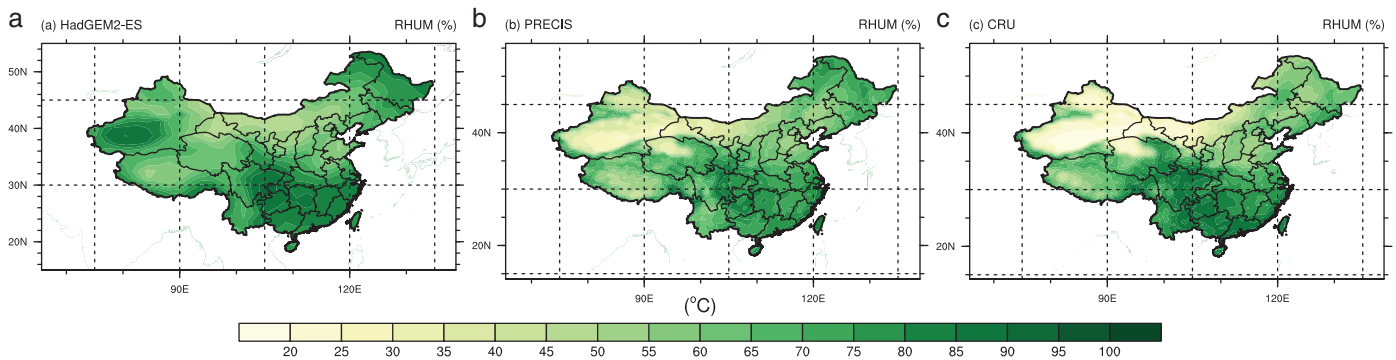


Figure 7. Spatial distributions of mean relative humidity (%) over China from HadGEM2-ES (a), PRECIS (b), and observations (CRU) (c) for 1976–2005.

strong reduction in modeled precipitation intensity with high temperatures is associated with a deficit in humidity (atmospheric moisture content), but this relationship is yet to be understood. Relations between temperature and humidity are difficult to assess because of an ambiguity of causes and effects, in particular over moisture-limited regions and the summer season (Trenberth & Shea, 2005). Most important is the dependency of both temperature and humidity on the atmospheric circulation conditions (Lenderink & van Meijgaard, 2009). The PRECIS model employs a closure of the convection scheme based on moisture convergence (Wilson et al., 2015). This closure led to a strong positive feedback with soil drying leading to a reduction in precipitation, opposing the results of HadGEM2-ES that gave rise to a negative soil moisture feedback. Despite the fact that extreme precipitation intensities over China are overestimated by PRECIS, it still produces more realistic relationship between temperature and RH, which is well reflected in the diagram (Figure 8). Therefore, the results exhibit a reference for PRECIS adding values to its driving GCM by capturing the relationship between temperature and RH in the land surface.

#### 4. Projections of Future Temperature and Humidity

Figure 9 shows the projected temperature changes relative to the baseline period for PRECIS under RCP4.5 and RCP8.5 scenarios for the period 2036–2065 (2050s) and the period 2070–2099 (2080s). Under RCP4.5, PRECIS projects general increases in the annual mean, maximum, and minimum temperatures over the whole China for both periods. It also can be found that the positive temperature changes are increasing in the mean temperature of days and nights from the 2050s to the 2080s. For both periods, there is no big difference between the mean minimum temperature and mean maximum temperature in terms of the warming magnitude. But the model tends to simulate warming spread to larger areas in the mean minimum temperature than those in the mean maximum temperature. PRECIS simulates that the northern subregions (Northwest China, Northcentral China, Northeast China, and Tibet) slightly warm more than southern subregion (South China) does. Under RCP8.5, PRECIS also projects warming across the landmass of China, while the warming degree is larger than the degree under RCP4.5 for each period. Especially in the 2080s, the warming in days' and nights' temperature became more significant with the increasing in the radiative forcing. It is also noted that contrast between the warming in mean maximum temperature and the minimum temperature is greater under RCP8.5 than RCP4.5 in the 2080s. Moreover, the warming in the northern subregions is higher than in the southern subregions concerning warming magnitude for both days' and nights' temperature in the 2080s. With the big difference between these areas, warming centers with significant temperature changes can be detected. At the late of the 21st century, there are two warming centers with changes greater than 6°C that can be detected in the mean maximum temperature namely, the northern parts of Northwest China and Northeast China. As for the mean minimum temperature, the areas with changes more than 6°C are all over the northern subregions, and only one warming center with changes >9°C can be found.

Figure 10 demonstrates the area averages of temperature changes for China and its five subregions. For both mean maximum and minimum temperatures, all China and its five subregions have positive changes under both RCPs for two future periods. Besides, four northern subregions have larger mean temperature changes than the one southern subregion. For Northwest, Central North, and Northwest China, the main

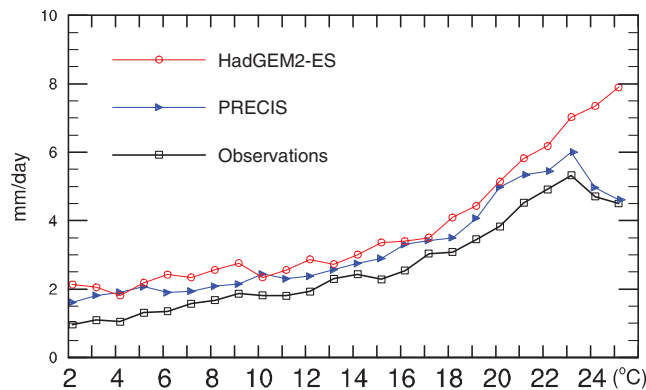
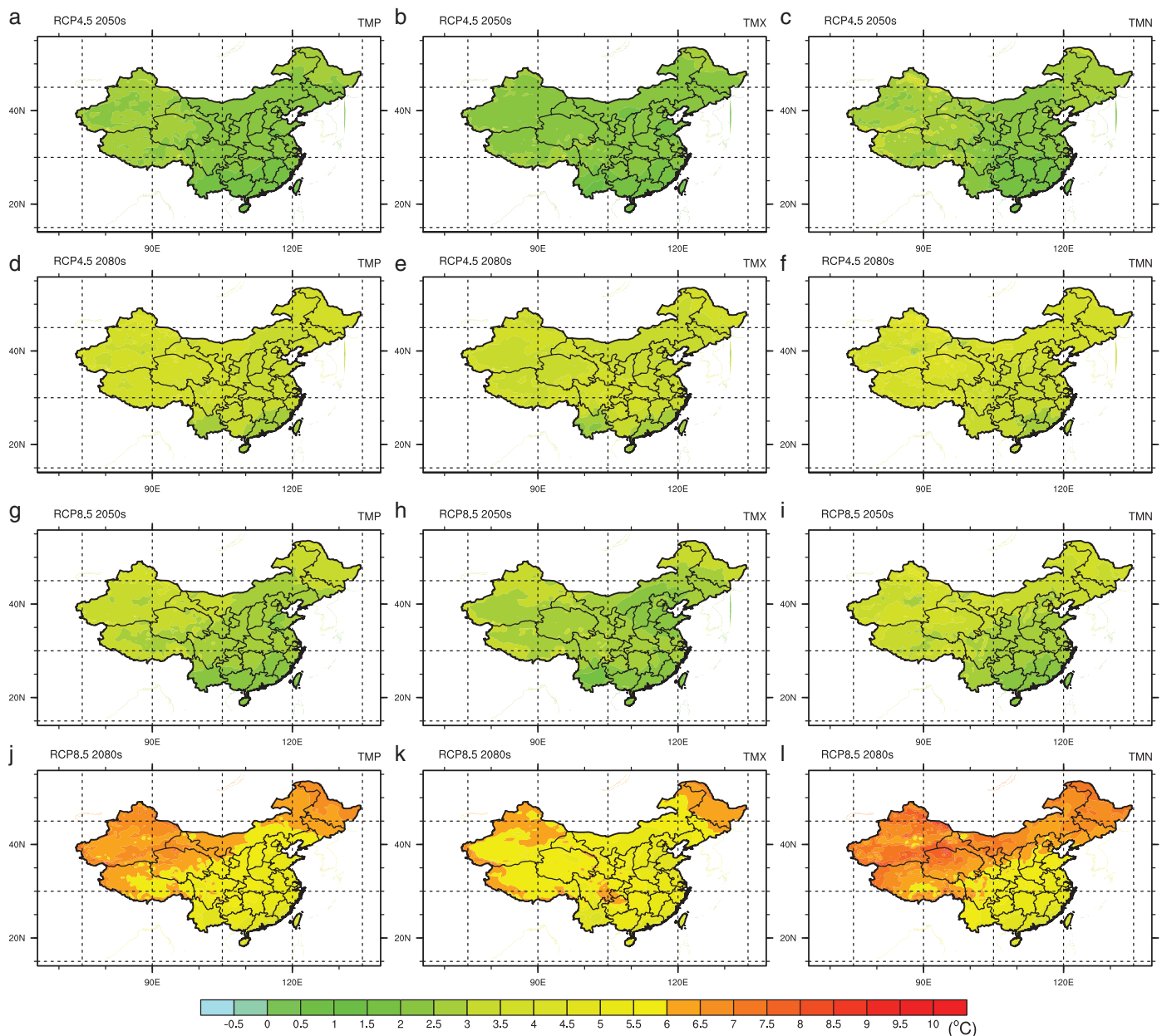


**Figure 8.** Dependencies of extreme percentiles (90th) of the distribution of daily precipitation on temperature in three data sets (HadGEM2-ES, PRECIS, and Observations).

reason why they have higher warming rate than the South China is that their relatively high latitudes make them receive more positive albedo-temperature feedback. As for Tibet, melting of the ice and snow cover in the high-elevation areas under warming climate increases water vapor which traps more heat in the surface, and makes the surface less reflective and adds to the warming effect (Wang et al., 2015a, 2015b). It is also apparent that warming in the mean temperature of nights is greater than the mean temperature of days (from 0.3 to 1.5°C). This warming trend agrees with the conclusion drew from Figure 7 that

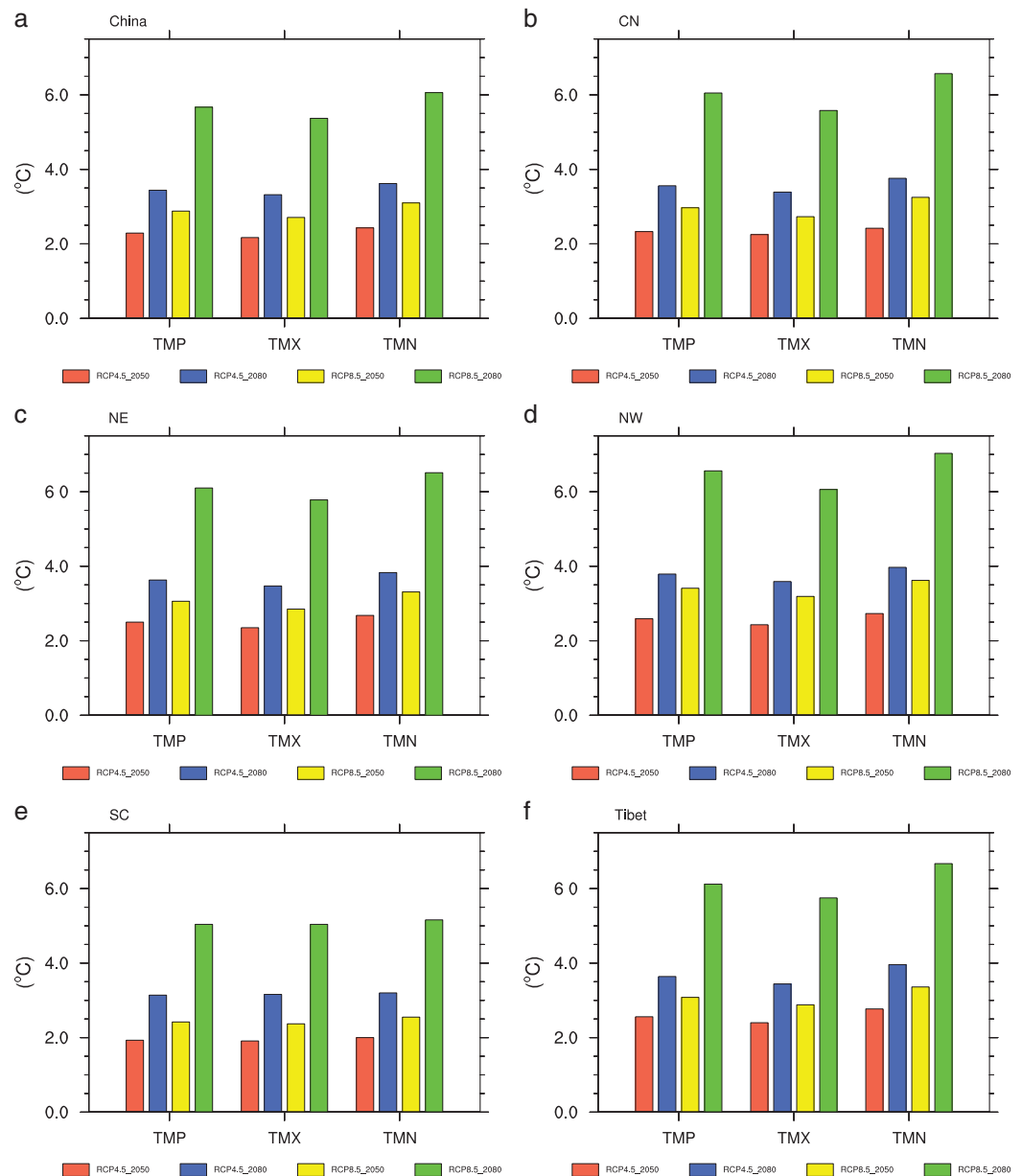
warming in the minimum temperature contributes more to the warming in the annual temperature than the maximum temperature does. It had been found that the greenhouse effect would be more effective and impedes radiation from escaping into space (Gong et al., 2014). Therefore, the minimum temperature would rise faster than the maximum temperature, and the difference between them (diurnal temperature) will be amplified with more greenhouse gas emission (Li et al., 2011). In detail, the annual mean temperature of China will increase 2.3°C in the 2050s and 3.4°C in the 2080s under RCP4.5, and 2.9°C in the 2050s and 5.7°C in the 2080s under RCP8.5. Among all five subregions, Northwest is expecting the largest warming for both the annual maximum and minimum temperature under both scenarios in both two future periods. In the 2080s, the increment of minimum temperature can reach 7.0°C under RCP8.5. The second largest warming will take place in Tibet and Northeast with increases both close to the temperature of Northwest regarding the annual mean maximum and minimum temperatures. South China will have the smallest warming for both days and nights' temperature under two different scenarios in both periods (1.9°C in the 2050s and 3.1°C in the 2080s under RCP4.5; 2.4°C in the 2050s and 5.0°C in the 2080s under RCP8.5 with respect to the annual mean temperature).

Figure 11 shows the projected changes relative to the reference period in the indices of temperature extremes over China under RCP4.5 and RCP8.5 for two future periods. Results for Summer Days have the maximum change takes place in the southern of South China, and the minimum change is in Tibet. Under stabilized radiative forcing scenario, the index's changes in the 2050s are relatively consistent with the changes in the 2080s. But the spatial distribution of the index shows noticeable changes between two periods under high concentration scenario. For a given future period, all five subregions will have more summer days than the reference period with the radiative forcing increases from RCP4.5 to RCP8.5. But the areas with maximum and minimum changes remain the same through the whole time. The pattern of Tropical Nights is consistent with that of Summer Days in terms of geographical differences in the index changes. The only difference is that the magnitude of index changes in Tropical Nights is smaller than that in Summer Days. TN90p presents the percentage of time where a daily minimum temperature in a time series is less than the 90th percentile of daily minimum temperature for the baseline period. Figure 11 show that the most significant increases in TN90p appear in the southern part of South China subregion. At the late 21st century, the increase can go up to 60% percentage under the high emission scenario. TX90p is defined as the percentage of time where a daily maximum temperature in a time series is less than the 90th percentile of daily maximum temperature for the baseline period. TX90p has the similar spatial distributions of the increases to TN90p with larger increases in southern subregion than in northern subregions, but the magnitude of increases is smaller for every scenario (only 46% under RCP8.5 in the 2080s). The geographical features of HWFI (Warm spell duration index: annual count of days with at least six consecutive days when daily maximum temperature >90th percentile of daily maximum temperature for the baseline period) have positive changes over China under any RCP for any period. The increase in HWFI is amplified by the increase in radiative forcing.



**Figure 9.** Spatial distributions of percentage changes for two future periods (2036–2065 relative to 1976–2005 and 2070–2099 relative to 1976–2005) of mean (TMP; a, d, g, j), maximum (TMX; b, e, h, k) and minimum (TMN; c, f, i, l) temperature ( $^{\circ}\text{C}$ ) as projected by PRECIS.

Regional statistics for projected indices of temperature extremes under RCP4.5 and RCP8.5 for two future periods are displayed in Figure 12. All the projected regional hot extreme events have the same geophysical distribution compared to the histogram for baseline period. From RCP4.5 to 8.5, both SU and TR are increasing with the radiative forcing increasing. Therefore, the whole nation will have hotter extreme events under RCP8.5 than RCP4.5. Moreover, the magnitudes of increase are relatively small between two RCPS in the 2050s when both RCPS have no significant difference in the radiative forcing. When comes to the 2080s, the magnitude of changes between two RCPS is larger than the 2050s. Despite the spatial distribution of the extreme events, what concerned mostly is the future changes of them relative to the baseline period. From Figure 12, we can see all values in SU and TR are positive. Therefore, China will have more summer days and tropical nights in the future. Regionally, South China has the largest increases in SU and TR. In opposite, Tibetan Plateau has the smallest increase in SU and TR. TN90p and TX90p have all values above 10% which



**Figure 10.** Future percentage changes (2036–2065 relative to 1976–2005 and 2070–2099 relative to 1976–2005) of mean (TMP), maximum (TMX) and minimum (TMN) temperature (°C) for PRECIS over China (a) and its five subregions (b–f) under RCP4.5 and RCP8.5.

mean the extremely high temperature above the 90th percentile of daily minimum and maximum temperature in the baseline period have more frequency to happen in the future. It is noted that TN90p's values out weight TX90p's. Future nights have more frequency of extremely high temperature than future days. Coinciding with the beforementioned two indices, China will experience more frequency of extremely high temperature with the radiative forcing increase. Additionally, the degree of changes in frequencies can also be amplified by increasing the radiative forcing. For instance, the increases in frequencies of TN90p under RCP8.5 are greater than the increases under RCP4.5 in the 2080s. The projected warm spell duration index follows the patterns derived from the baseline period concerning spatial distribution. Same to other indices, HWFI has positive changes under no matter which scenarios. With the radiative forcing increased, China will have a longer duration for the warm spell. For five subregions, South China have the largest change in HWFI and Northeast has the smallest.

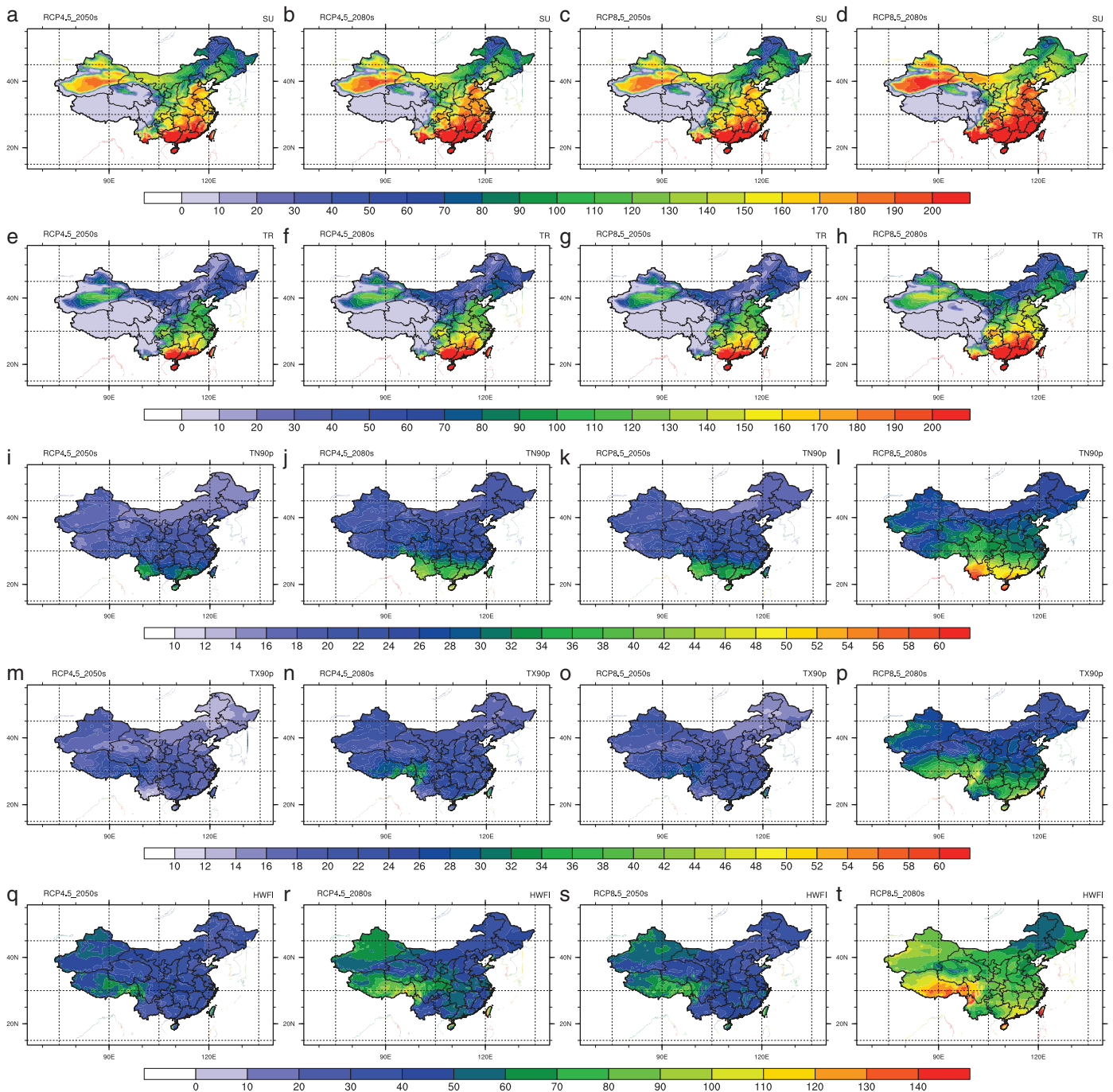


**Figure 11.** Spatial distributions of projected indices of high-temperature extremes (SU, day; TR, day; TN90p, %; TX90p, %; HWFI, day) over China under RCP4.5 and RCP8.5 for two future periods (2036–2065 and 2070–2099).

With global warming in the future, China is likely to experience more number of extremely hot days, more frequent high-temperature extremes, and longer duration of warm spell than the baseline period. We can conclude it from investigating the five high-temperature indices that the frequency of high-temperature extremes can be changed up to 40% and the duration can be changed up to 150% in China by the increased radiative forcing in the end of 21st century. Regionally, South China has the largest increases in all indices of high-temperature extreme and the smallest changes in the mean, maximum, and minimum temperatures. This implicates that the future climate in South China will be changing more violent than the

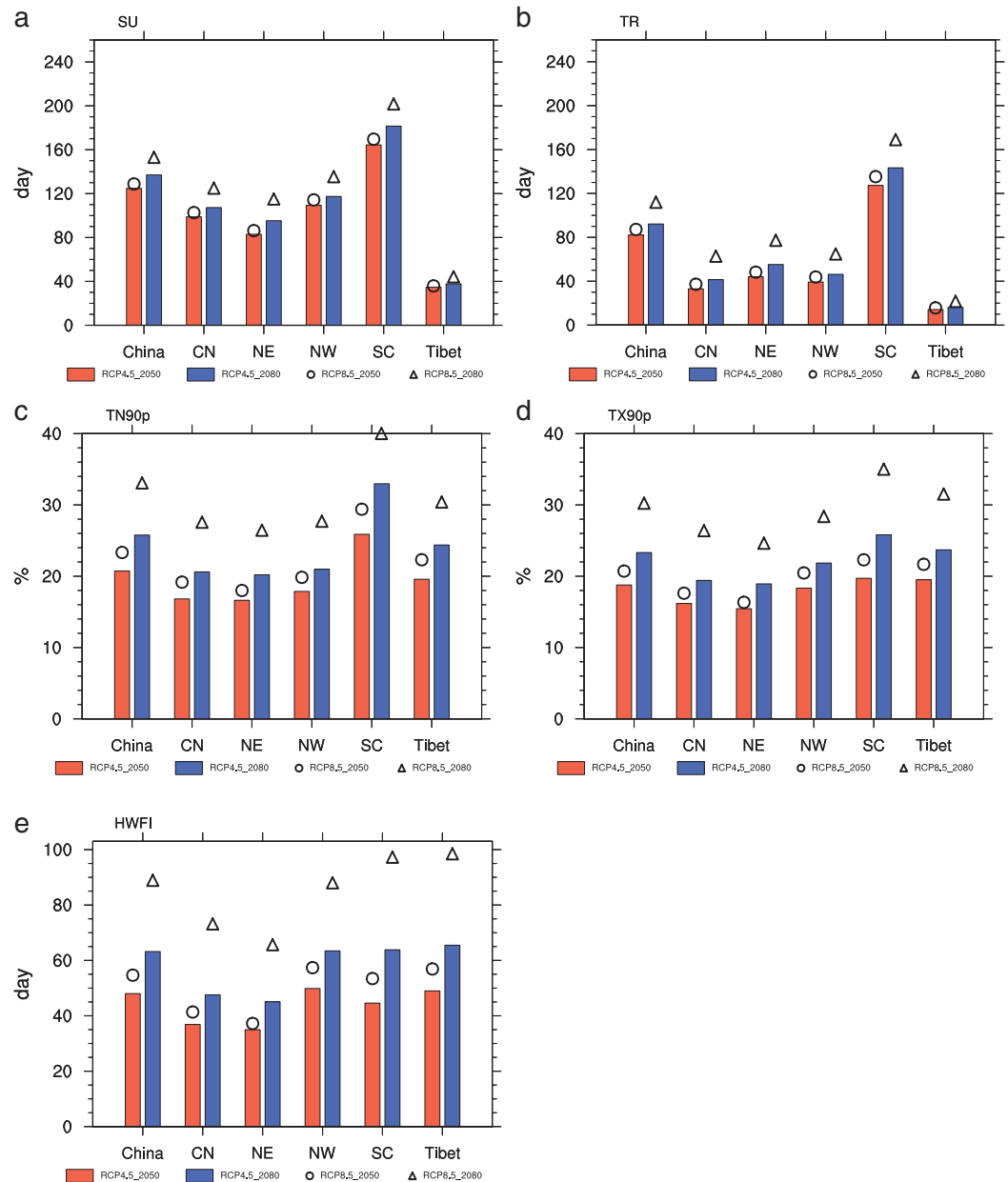


**Figure 12.** Regional averages for indices of annual mean high-temperature extremes (SU, day; TR, day; TN90p, %; TX90p, %; HWFI, day) over China and its five subregions for two future periods (2036–2065 and 2070–2099).

reference period. South China is expecting more high-temperature extreme events in summer and more low-temperature extreme events in winter.

As shown in Figure 13, the distribution of future RH generally follows the spatial pattern in the reference period, which is relative low value in northwest China and increasing southeastward. Comparing to temperatures, RH is less affected by the changes in radiative forcing. Despite some differences in details, RH remains same and does not have any notable changes in the magnitude. To investigate into the magnitude, the projected change in the future RH was displayed in Figure 14 under the RCPs scenario for two periods relative to the baseline period. Under the both scenarios, PRECIS projects that RH will increase over northwest, north-central, and southwest China. Especially, PRECIS tends to enhance the increasing conditions over these three subregions with radiative forcing increasing for both periods. As for the areas with decreasing RH marked as red in the maps, they are two river basins, Amur River basin in northeast China and Yangtze basin in South

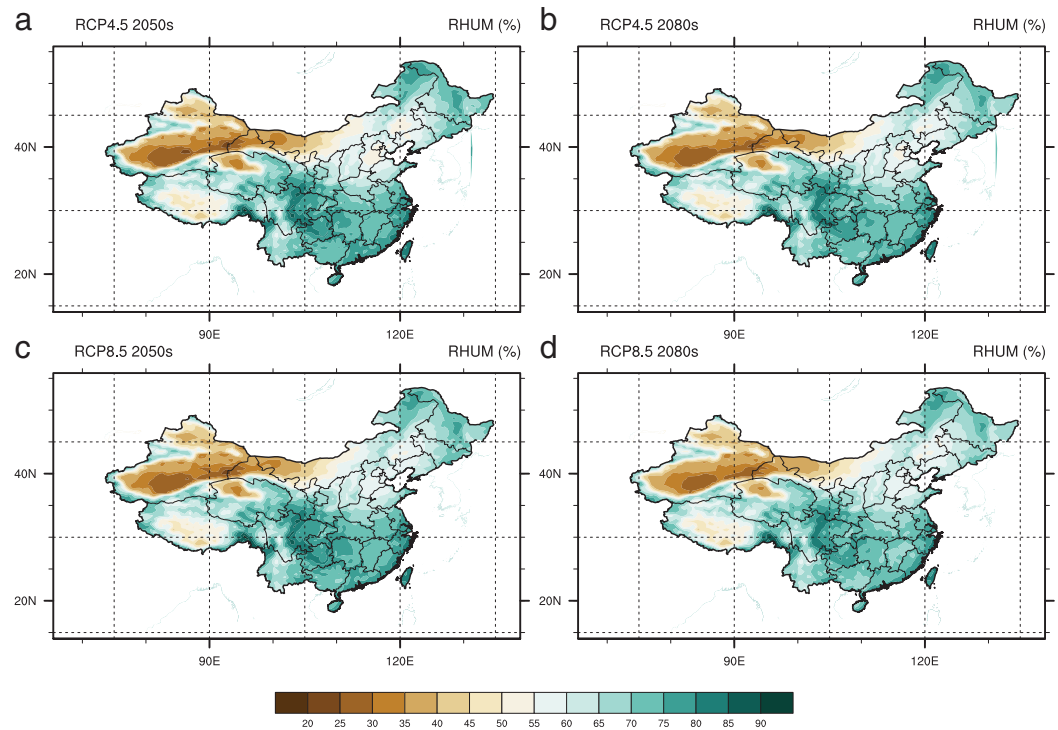


**Figure 13.** Spatial distributions of percentage changes for two future periods (2036–2065 relative to 1976–2005 and 2070–2099 relative to 1976–2005) of mean relative humidity (unit: %) as projected by PRECIS. (a) RCP4.5 2050s, (b) RCP4.5 2080s, (c) RCP4.5 2080s, (d) RCP8.5 2080s.

China. Similarly, PRECIS tends to enhance the decreasing trend over both basins with increases in radiative forcing for both future periods. This may be related to the Asian monsoon changed by climate change, because climate over both basins is controlled by the Asian monsoon. From Zou et al.'s study, enhanced warming under climate change reduces the thermal contrast between the Asian land mass and neighboring oceans. Monsoon-affected areas will experience a weak monsoon, which prevents warm-humid air from oceans (Zou et al., 2016). Despite all the changes in China, the maximum magnitude of changes is only 8% from the RH in the baseline period. The changes in RH are not as obvious as temperatures under climate change. Therefore, we can conclude that RH is not as sensitive as temperatures are to the increases in the radiative forcing.

Dew point temperature is chosen to demonstrate how the combination effects of temperature and RH will change under climate change, because it is defined as the temperature to which air must be cooled (at constant water vapor content and constant pressure) to reach saturation. The dew point temperature ( $td$ ) was computed from the RH ( $rh$ ) and temperature ( $T$ ) by the conversion equation from the Magnus–Tetens Approximation (Lawrence, 2005). This approximation provides a maximum error of 0.1% for temperatures between  $-45^{\circ}\text{C}$  and  $60^{\circ}\text{C}$ , and RH between 1% and 100%.

$$td = \frac{B \times \left[ \ln \left( \frac{rh}{100} \right) + \frac{A \times T}{B+T} \right]}{A - \ln \left( \frac{rh}{100} \right) - \frac{A \times T}{B+T}}$$

$$A = 17.625$$

$$B = 243.04^{\circ}\text{C}$$

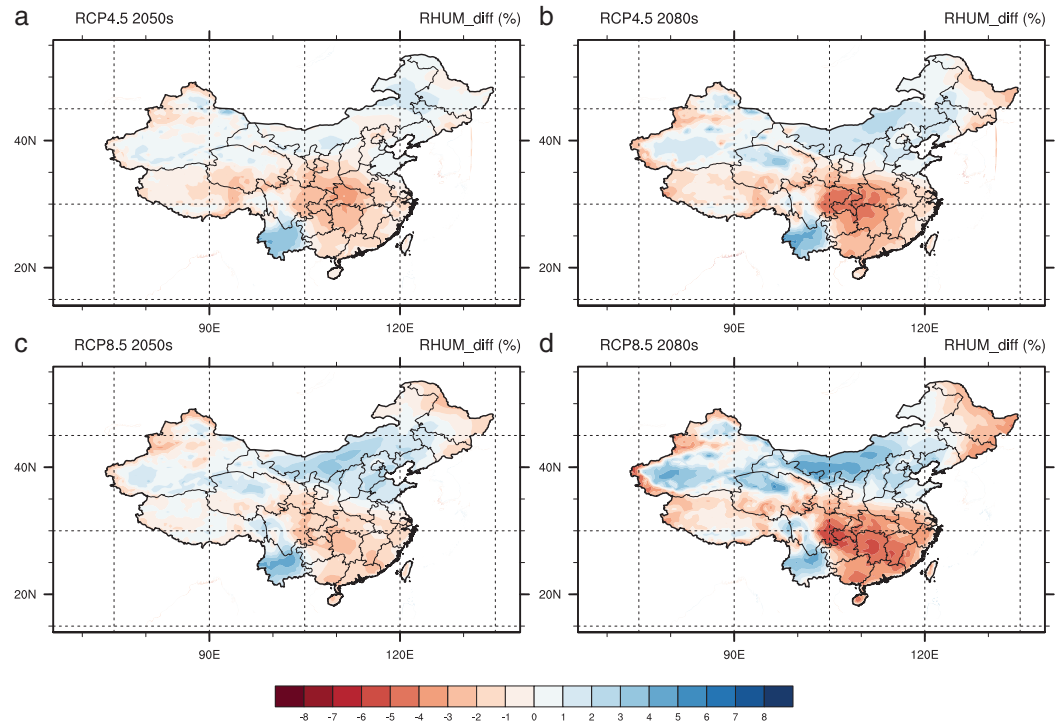


**Figure 14.** Future percentage changes (2036–2065 relative to 1976–2005 and 2070–2099 relative to 1976–2005) of mean relative humidity (%) for PRECIS over China under RCP4.5 (a, b) and RCP8.5 (c, d).

As the measurement of dew pint related to humidity, a higher dew point temperature means a temperature comes with more moisture. In the Introduction section, we discussed that high humidity in the atmosphere will retarded the perspiration process. The discomfort of human bodies increases with the unevaporated perspiration. Studies found that most inhabited areas will consider the dew point of 21°C as the threshold for discomfort and 7–20°C as the comfortable interval (Robinson, 2000). In Figure 15, dew points above the threshold of 21°C are marked with red and dew points between 7 and 20°C are marked with yellow. Yellow color covers the most parts of South China and only the southern island (Hainan Province) is covered by the red for the baseline period. With the radiative forcing increasing from RCP4.5 to 8.5, the area covered with yellow shrinks from the southern part of South China where has been taken over by the red color for both future periods. By the end of the 21st century, the red spreads to the most parts of Guangdong Province, southern parts of Guangxi and Taiwan Provinces under RCP8.5. But the northern boundary of the yellow area remains unchanged under RCPs through the whole time. Compared to the reference period, the changes in the dew point temperature over the South China are 1.3°C under RCP 4.5 in the 2050s, 2.4°C under RCP4.5 in the 2080s, 1.9°C under RCP8.5 in the 2050s, and 4.1°C under RCP8.5 in the 2080s. Considering the area averaged dew point temperature over South China is 11°C for the period from 1976 to 2005, the combination effects of high-temperatures and RH are substantially smaller than generally anticipated for China (Fischer & Knutti, 2013). The reason behind this finding is that the model that projects greater warming does not show a correlated strong RH increase in the RH.

### 5. Conclusions

In this study, the PRECIS model is employed to investigate the temperature extremes and RH response to climate change at a national level with consideration of the interconnection among climate variables. In detail, we investigated the projected temperature extremes, RH and dew point temperatures for China under different scenarios for two future periods. We first examined the selected RCM's skill in reproducing the historical climate over China for the baseline period. A reasonable reproduction of historical climate was obtained through the validation with the observation data set in terms of the temperatures, humidity and the relationship between them. After the validation, a plausible range of future temperatures and

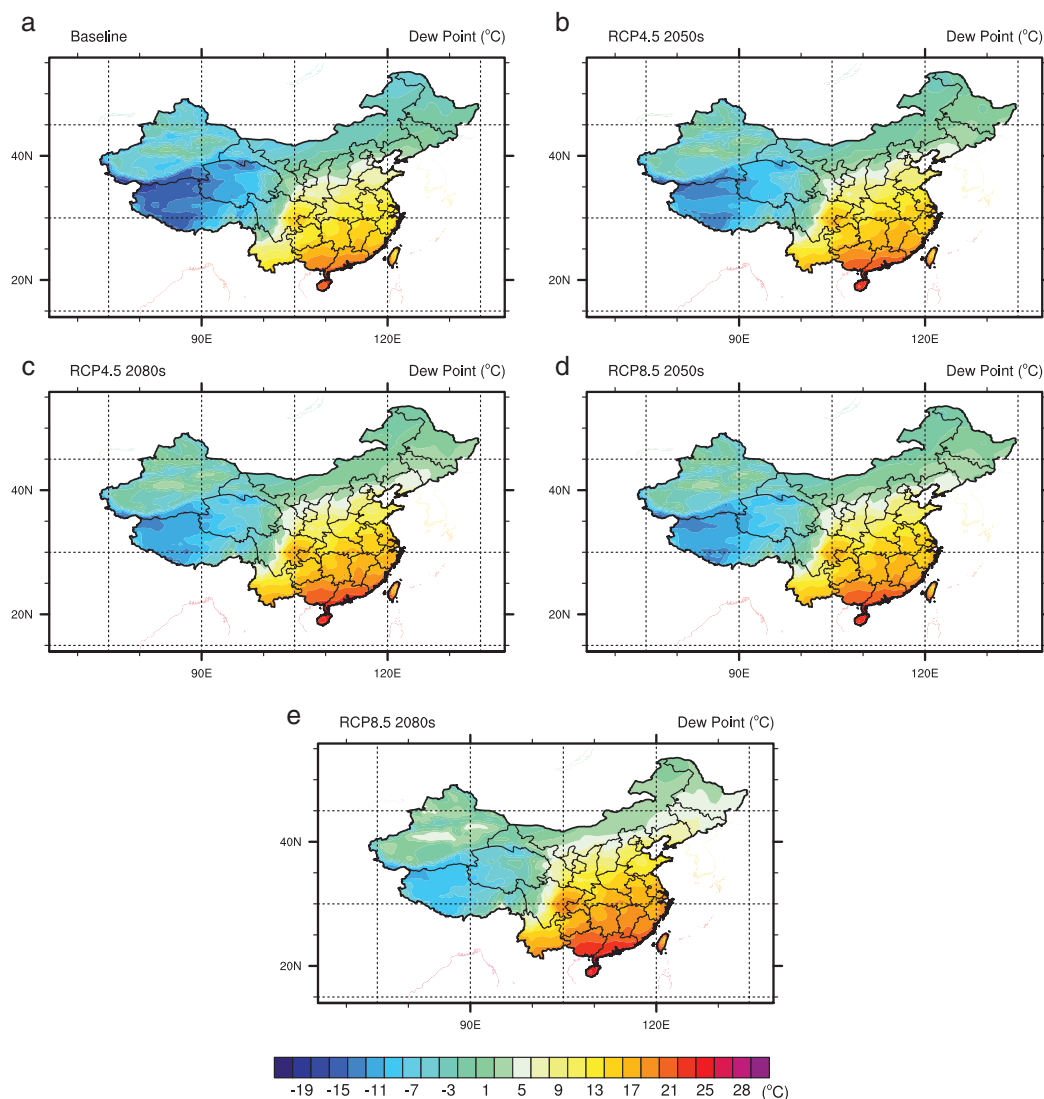


**Figure 15.** Spatial distributions of projected dew point temperatures ( $^{\circ}\text{C}$ ) over China under RCP4.5 and RCP8.5 for two future periods (2036–2065 and 2070–2099). (a) Baseline, (ba) RCP4.5 2050s, (c) RCP4.5 2080s, (d) RCP4.5 2080s, and (e) RCP8.5 2080s

RH were generated under RCPs to build the foundation for investigating how the joint projections of high temperatures and RH response to climate change at a fine spatial resolution.

The PRECIS model projects the annual mean temperature of China will increase up to  $6^{\circ}\text{C}$  under high radiative forcing scenario at the end of 21st century. Opposite to the significantly change in the temperature, the maximum magnitude of changes in RH is only 8% from the value in the baseline period. The dew point temperature, which is chosen to demonstrate how the combination effects of high temperature and RH, is projected to increase  $4.1^{\circ}\text{C}$  over South China (the concerning area with high temperature compounded by high humidity) under RCP8.5 in the 2080s. As the area-averaged dew point temperature over South China is  $11^{\circ}\text{C}$  for the period from 1976 to 2005, the future dew point temperature is still within the comfortable interval even under the worst scenario. Therefore, the combination effects of high temperatures and RH are substantially smaller than generally anticipated for China. This is because that the model does not project the increase in RH as great as the increase in temperatures. Even though the impact-relevant metric like the dew point temperature is not projected as bad as the generally anticipated, China is still expected to have more number of extremely hot days, more frequent high-temperature extremes, and longer duration of warm spell than before. By investigating the five high-temperature indices, we found that the frequency

of high-temperature extremes can be changed up to 40% and the duration can be changed up to 150% in China by the increased radiative forcing in the end of 21st century. Regionally, extra cautions need to be given to South China, as it has the smallest changes in the mean, maximum and minimum temperatures while the largest increases in all five high-temperature indices. Consequently, the climate over South China for two future periods will be changing more drastically than the baseline period. South China is expecting more high-temperature extreme events in summer and more low-temperature extreme events in winter.

### Acknowledgments

This research was supported by the China Scholarship Council, the Natural Sciences Foundation (51190095, 51225904), the Program for Innovative Research Team in University (IRT1127), the 111 Project (B14008), and the Natural Science and Engineering Research Council of Canada. Readers can find the data that support or underlie the conclusions presented in Climate Change Data Portal for China (<http://chinaccdd.org/>).

### References

- Beniston, M. (2009). Trends in joint quantiles of temperature and precipitation in Europe since 1901 and projected for 2100. *Geophysical Research Letters*, *36*, L07707. <https://doi.org/10.1029/2008GL037119>.
- Chen, K., Bi, J., Chen, J., Chen, X., Huang, L., & Zhou, L. (2015). Influence of heat wave definitions to the added effect of heat waves on daily mortality in Nanjing, China. *Science of the Total Environment*, *506*, 18–25. <https://doi.org/10.1016/j.scitotenv.2014.10.092>
- Chen, X., & Zhou, T. (2017). Relative contributions of external SST forcing and internal atmospheric variability to July–August heat wave over the Yangtze River valley during 1979–2014. *Climate Dynamics*. <https://doi.org/10.1007/s00382-017-3871-y>
- Cheng, G., Huang, G., Dong, C., Zhu, J., Zhou, X., & Yao, Y. (2017). Recursive multivariate principal-monotonicity inferential climate downscaling. *Quarterly Journal of the Royal Meteorological Society*. <https://doi.org/10.1002/qj.3126>
- Collins, W., Bellouin, N., Doutriaux-Boucher, M., Gedney, N., Hinton, T., Jones, C., ... Kim, J. (2008). Evaluation of the HadGEM2 model. Met Office Hadley Centre Technical Note no. HCTN 74, Met Office, FitzRoy Road, Exeter. Retrieved from <http://www.metoffice.gov.uk/publications/HCTN/index.html>.
- Ding, T., Qian, W., & Yan, Z. (2010). Changes in hot days and heat waves in China during 1961–2007. *International Journal of Climatology*, *30*(10), 1452–1462. <https://doi.org/10.1002/joc.1989>
- Fang, S., Qi, Y., Han, G., & Zhou, G. (2015). Changing trends and abrupt features of extreme temperature in mainland China during 1960 to 2010. *Earth Systems Dynamics and Discussions*, *6*, 979–1000. <https://doi.org/10.5194/esdd-6-979-2015>
- Fang, X., Wang, A., Fong, S., Lin, W., & Liu, J. (2008). Changes of reanalysis-derived northern hemisphere summer warm extreme indices during 1948–2006 and links with climate variability. *Global and Planetary Change*, *63*(1), 67–78. <https://doi.org/10.1016/j.gloplacha.2008.06.003>
- Feng, J., Wang, Y., Ma, Z., & Liu, Y. (2012). Simulating the regional impacts of urbanization and anthropogenic heat release on climate across China. *Journal of Climate*, *25*(20), 7187–7203. <https://doi.org/10.1175/JCLI-D-11-00333.1>
- Feng, S., Hu, Q., & Qian, W. (2004). Quality control of daily meteorological data in China, 1951–2000: A new dataset. *International Journal of Climatology*, *24*, 853–870. <https://doi.org/10.1002/joc.1047>
- Fischer, E. M., & Knutti, R. (2013). Robust projections of combined humidity and temperature extremes. *Nature Climate Change*, *3*, 126–130. <https://doi.org/10.1038/nclimate1682>
- Flato, G., Abiodun, B., Braconnot, P., Chou, S. C., ... Collins, W. (2013). Evaluation of Climate Models. In: *Climate Change 2013: The Physical Science Basis. Contribution of Working Group I to the Fifth Assessment Report of the Intergovernmental Panel on Climate Change*. Cambridge, UK: Cambridge University Press.
- Frich, P., Alexander, L. V., Della-Marta, P., Gleason, B., Haylock, M., Klein Tank, A. M. G., & Peterson, T. (2002). Observed coherent changes in climatic extremes during the second half of the twentieth century. *Climate Research*, *19*, 193–212. <https://doi.org/10.3354/cr019193>
- Goff, J. A., & Gratch, S. (1946). Low-pressure properties of water from –160° to 212°F. Transactions of the American Society of Heating and Ventilating Engineers: 52nd annual meeting of the American Society of Heating and Ventilating Engineers. *ASHVE*, New York, 95–122.
- Gong, H., Wang, L., Chen, W., Wu, R., Wei, K., & Cui, X. (2014). The climatology and interannual variability of the East Asian winter monsoon in CMIP5 models. *Journal of Climate*, *27*(4), 1659–1678. <https://doi.org/10.1175/JCLI-D-13-00039.1>
- Harris, I., Jones, P. D., Osborn, T. J., & Lister, D. H. (2014). Updated high-resolution grids of monthly climatic observations – The CRU TS3.10 dataset. *International Journal of Climatology*, *34*, 623–642. <https://doi.org/10.1002/joc.3711>
- Hewitson, B., Janetos, A. C., Carter, T. R., Giorgi, F., Jones, R. G., ... van Aalst, M. (2014). Regional context. In V. R. Barros, et al. (Eds.), *Climate Change 2014: Impacts, Adaptation, and Vulnerability. Part B: Regional Aspects. Contribution of Working Group II to the Fifth Assessment Report of the Intergovernmental Panel on Climate Change* (pp. 1133–1197). Cambridge, UK: Cambridge University Press.
- Isaac, V., & van Wijngaarden, W. A. (2012). Surface water vapor pressure and temperature trends in North America during 1948–2010. *Journal of Climate*, *25*, 3599–3609. <https://doi.org/10.1175/JCLI-D-11-00003.1>
- Jones, R., Noguer, M., Hassell, D., Hudson, D., Wilson, S., Jenkins, G., & Mitchell, J. (2004). *Generating high resolution climate change scenarios using PRECIS ()*. Exeter, UK: Met Office Hadley Centre 40 pp.
- Lawrence, M. G. (2005). The relationship between relative humidity and the Dewpoint temperature in moist air: A simple conversion and applications. *Bulletin of the American Meteorological Society*, *86*, 225–233. <https://doi.org/10.1175/BAMS-86-2-225>
- Lenderink, G., & van Meijgaard, E. (2009). Reply to: Unexpected rise in extreme precipitation caused by a shift in rain type. *Nature Geoscience*, *2*, 373. <https://doi.org/10.1038/ngeo524>
- Li, H., Feng, L., & Zhou, T. (2011). Multi-model projection of July–August climate extreme changes over China under CO<sub>2</sub> doubling. Part II: Temperature. *Advances in Atmospheric Sciences*, *28*, 448. <https://doi.org/10.1007/s00376-010-0052-x>
- Li, Q., Zhang, L., Xu, W., Zhou, T., Wang, J., Zhai, P., & Jones, P. (2017). Comparisons of time series of annual mean surface air temperature for China since the 1900s: Observations, model simulations and reanalysis. *Bulletin of American Meteorological Society*. <https://doi.org/10.1175/BAMS-D-16-0092.1>
- Lin, Z., Yu, Z., Zhang, H., & Wu, C. (2016). Quantifying the attribution of model bias in simulating summer hot days in China with IAP AGCM 4.1. *Atmospheric and Oceanic Science Letters*, *9*(6), 436–442. <https://doi.org/10.1080/16742834.2016.1133071>
- List, R. J. (2000). *Smithsonian Meteorological Tables* (6th ed., p. 540). Washington, DC: Smithsonian Institution.
- Ma, S., Zhou, T., Stone, D., Angellil, O., & Shiogama, H. (2017). Attribution of the July–August 2013 heat event in central and eastern China to anthropogenic greenhouse gas emissions. *Environmental Research Letters*, *12*, 054020. <https://doi.org/10.1088/1748-9326/aa69d2>
- Moss, R. H., Edmonds, J. A., Hibbard, K. A., Manning, M. R., Rose, S. K., van Vuuren, D. P., ... Wilbanks, T. J. (2010). The next generation of scenarios for climate change research and assessment. *Nature*, *463*(7282), 747–756. <https://doi.org/10.1038/nature08823>
- Murray, F. W. (1967). On the computation of saturation vapor pressure. *Journal of Applied Meteorology*, *6*, 203–204. [https://doi.org/10.1175/1520-0450\(1967\)006<0203:OTCOSV>2.0.CO;2](https://doi.org/10.1175/1520-0450(1967)006<0203:OTCOSV>2.0.CO;2)

- Ren, G., & Zhou, Y. (2014). Urbanization effect on trends of extreme temperature indices of national stations over mainland China, 1961–2008. *Journal of Climate*, 27(6), 2340–2360. <https://doi.org/10.1002/2015GL065973>
- Robinson, P. J. (2000). Temporal trends in United States dew point temperatures. *International Journal of Climatology*, 20, 985–1002. [https://doi.org/10.1002/1097-0088\(200007\)20:9<985::AID-JOC513>3.0.CO;2-W](https://doi.org/10.1002/1097-0088(200007)20:9<985::AID-JOC513>3.0.CO;2-W)
- Sperber, K. R., Annamalai, H., Kang, I. S., Kitoh, A., Moise, A., Turner, A., ... Zhou, T. (2013). The Asian summer monsoon: An intercomparison of CMIP5 vs. CMIP3 simulations of the late 20th century. *Climate Dynamics*, 41(9–10), 2711–2744. <https://doi.org/10.1007/s00382-012-1607-6>
- Taylor, K. E. (2001). Summarizing multiple aspects of model performance in a single diagram. *Journal of Geophysical Research*, 106, 7183–7192. <https://doi.org/10.1029/2000JD900719>
- Tebaldi, C., & Sansó, B. (2009). Joint projections of temperature and precipitation change from multiple climate models: a hierarchical Bayesian approach. *Journal of the Royal Statistical Society: Series A (Statistics in Society)*, 172, 83–106. <https://doi.org/10.1111/j.1467-985X.2008.00545.x>
- Trenberth, K. E., & Shea, D. J. (2005). Relationships between precipitation and surface temperature. *Geophysical Research Letters*, 32, L14703. <https://doi.org/10.1029/2005GL022760>
- Utsumi, N., Seto, S., Kanae, S., Maeda, E. E., & Oki, T. (2011). Does higher surface temperature intensify extreme precipitation? *Geophysical Research Letter*, 38, L16708. <https://doi.org/10.1029/2011GL048426>
- Wang, W. G., & Zheng, G. G. (2012). *Annual Report on Actions to Address Climate Change (2012): Climate Finance and Low Carbon Development (in Chinese)* (). Beijing: Social Sciences Academic Press 306 pp.
- Wang, X., Huang, G., Lin, Q., Nie, X., & Liu, J. (2015a). High-resolution temperature and precipitation projections over Ontario, Canada: A coupled dynamical-statistical approach. *Quarterly Journal of the Royal Meteorological Society*, 141, 1137–1146. <https://doi.org/10.1002/qj.2421>
- Wang, X., Li, G., Liu, L., Westerdahl, D., Jin, X., & Pan, X. (2015b). Effects of extreme temperatures on cause-specific cardiovascular mortality in China. *International Journal of Environmental Research and Public Health*, 12(12), 16136–16156. <https://doi.org/10.3390/ijerph121215042>
- Wang, X., Huang, G., & Liu, J. (2014). Projected increases in near-surface air temperature over Ontario, Canada: A regional climate modeling approach. *Climate Dynamics*, 45, 1381–1393. <https://doi.org/10.1007/s00382-014-2387-y>
- Watterson, I. G., & Whetton, P. H. (2011). Distributions of decadal means of temperature and precipitation change under global warming. *Journal of Geophysical Research*, 116, D07101. <https://doi.org/10.1029/2010JD014502>
- Wilson, W., D. Hassell, D. Hein, C. Wang, S. Tucker, R. Jones, and R. Taylor (2015), Technical manual for PRECIS: The Met Office Hadley Centre regional climate modelling system Version 2.0.0. Retrieved from [www.metoffice.gov.uk/precis](http://www.metoffice.gov.uk/precis).
- Xu, Y., Gao, X. J., Shen, Y., Xu, C. H., Shi, Y., & Giorgi, F. (2009). A daily temperature dataset over China and its application in validating a RCM simulation. *Advances in Atmospheric Sciences*, 26(4), 763–772. <https://doi.org/10.1007/s00376-009-9029-z>
- Xu, Y., Zhang, Y., Lin, E., Lin, W., Dong, W., Jones, R., ... Wilson, S. (2006). Analyses on the climate change responses over China under SRES B2 scenario using PRECIS. *Chinese Science Bulletin*, 51, 2260–2267. <https://doi.org/10.1007/s11434-006-2099-8>
- Yan, D., Werners, S., Ludwig, F., & Huang, H. (2015). Hydrological response to climate change: The Pearl River, China under different RCP scenarios. *Journal of Hydrology: Regional Studies*, 4(B), 228–245. <https://doi.org/10.1016/j.ejrh.2015.06.006>
- Zhou, T., Song, F., & Chen, X. (2013). Historical evolutions of global and regional surface air temperature simulated by FGOALS-s2 and FGOALS-g2: How reliable are the model results? *Advances in Atmospheric Sciences*, 30(3), 638–657. <https://doi.org/10.1007/s00376-013-2205-1>
- Zhu, J., Huang, G., Wang, X., Cheng, G., & Wu, Y. (2017). High-Resolution Projections of Mean and Extreme Precipitations over China through PRECIS under RCPs. *Climate Dynamics*. <https://doi.org/10.1007/s00382-017-3860-1>.
- Zou, L., Zhou, T., & Peng, D. (2016). Dynamical downscaling of historical climate over CORDEX East Asia domain: A comparison of regional ocean-atmosphere coupled model to stand-alone RCM simulations. *Journal of Geophysical Research – Atmospheres*, 121, 1442–1458. <https://doi.org/10.1002/2015JD023912>